Synthesis and Characterizations of Nanosized Iron(II) Hydroxide and Iron(II) Hydroxide/Poly(vinyl alcohol) Nanocomposite

M. Fathima Parveen,[1] S. Umapathy,[2] V. Dhanalakshmi,[3] R. Anbarasan[4]

[1]*Department of Physics, Hajee Karutha Rowther Howdia College, Uthamapalayam 625 533, Tamil Nadu, India*
[2]*School of Physics, Madurai Kamaraj University, Madurai 625 021, Tamil Nadu, India*
[3]*Department of Polymer Technology, KCET 626 001, Tamil Nadu, India*
[4]*Department of Mechanical Engineering, MEMS Thermal Control Lab, National Taiwan University, Taipei 10617, Taiwan, Republic of China*

Received 28 August 2009; accepted 18 February 2010
DOI 10.1002/app.32296
Published online 7 June 2010 in Wiley InterScience (www.interscience.wiley.com).

ABSTRACT: Nanosized $Fe(OH)_2$ was synthesized by a coprecipitation method. Peaks between 500 and 1250 cm^{-1} in Fourier transform infrared (FTIR) spectroscopy confirmed the presence of metal hydroxide stretching. X-ray diffraction showed the suppressed crystalline system of $Fe(OH)_2$/aniline (ANI) due to the presence of a higher weight percentage of the dispersing agent, ANI. Thermogravimetric analysis implied that 75.5 wt % of residue remained up to 800°C. High resolution transmission electron microscope (HRTEM) analysis of $Fe(OH)_2$/ANI revealed that its size ranged from 10 to 50 nm with a rod-like morphology. Scanning electron microscopy implied that pristine $Fe(OH)_2$ had a nanotriangular platelet morphology, and a higher weight percentage of dispersing agent intercalated with $Fe(OH)_2$ had a spheroid with an agglomerated structure. The (UV–visible) spectrum implied the presence of Fe^{2+} ions at 326 nm and the existence of an amino group intercalated with $Fe(OH)_2$ showed a sharp peak at 195 nm, the intensity of which increased with increasing intercalated dispersing agent weight percentage. Photoluminescence showed that ANI-intercalated $Fe(OH)_2$ showed a lesser intensity than the pristine $Fe(OH)_2$. © 2010 Wiley Periodicals, Inc. J Appl Polym Sci 118: 1728–1737, 2010

Key words: composites; differential scanning calorimetry (DSC); FTIR; nanocomposites

INTRODUCTION

For the past few decades, scientists have been using a technique to isolate ferrous materials from mixtures specially based on their magnetic properties. Nanosized magnetic materials with a large surface area and low material density could serve as an ideal building blocks for the fabrication of light-weight structural materials and for catalysis, nanoelectronics, drug-delivery applications,[1] magnetic resonance imaging, and cancer therapy.[2] Polymer-coated materials, particularly, biocompatible polymers coated with nanomagnetic materials, act together in cancer treatment as drug carrier/imaging agents. The key idea is a nanomagnetic material that can specifically target cancer cells with its bulk because of its active surface area.[3] Such materials with magnetic properties have been synthesized by many techniques. Let us review the literature available regarding the synthesis and characterization of such magnetic materials. Recently, Zhang et al.[4] used a hydrothermal method under oxygen-free condition for the synthesis of magnetic materials. Ohtsuka et al.,[5] with tetrasilisic mica intercalation, synthesized ferrous hydroxide. $Fe(OH)_2$-based LDH was synthesized by a sol–gel method and made into a composite with EVA copolymer.[6] Iron oxide hydroxide was synthesized by a coprecipitation method and used as a catalyst for the reduction of nitro groups into amino groups.[7] In 2001, Jung et al.[8] synthesized amorphous iron hydroxide, and its agglomerated structure was analyzed by the SALLS method. Iron hydroxide colloidal precipitates were used to remove heavy metals in effluent water.[9] $Fe(OH)_3$ was used to synthesize Co(II)–Fe(III) hydroxide carbonate.[10] Iijima et al.[11] synthesized surfactant-controlled iron hydroxide nanoparticles. Schwartz et al.[12] described various acid-encapsulated $Fe(OH)_3$'s. Yeung et al.[13] synthesized and characterized $Fe(OH)_3$. They synthesized $Fe(OH)_3$ by the oxidation of $FeSO_4$ in acidic medium, and they characterized the same by DTA, magnetic susceptibility,

Correspondence to: R. Anbarasan (anbu_may3@yahoo.co.in).

Mossbauer spectroscopy, particle size determination, X-ray diffraction (XRD), and electron microscopy techniques. In a thorough literature survey, we could not find many reports available for the synthesis, characterization, and application of nanosized $Fe(OH)_2$. In this investigation, we took that job as a challenge and successfully synthesized $Fe(OH)_2$ in nanosize and characterized it by many analytical techniques, and its nanocomposite with poly(vinyl alcohol) (PVA) was studied for the first time. The academic reason behind this investigation was that when a polymer-coated nanomagnetic material is prepared, the nanosized material due to its active surface area will alter the structure of polymer during drug-delivery applications. Our actual intention was to study the effect of nanosized materials on the structure of the polymer during drug-delivery applications in an aqueous medium quantitatively with Fourier transform infrared (FTIR) spectroscopy.

EXPERIMENTAL

Materials

Aniline [ANI; analar reagent (AR), Merck, India] was purified by distillation before use. Ferrous sulfate (Reachem, AR, India) and sodium hydroxide (Reachem, AR) were purchased and used as received. Double-distilled (DD) water was used for solution preparation purposes. PVA (S. D. Fine Chemicals, India) with a molecular weight of 125,000 (85% hydrolyzed) was used as received.

Methods

Synthesis of the nanosized $Fe(OH)_2$ and its hybrid

The procedure is briefly explained here. Ferrous sulfate (2.78 g) was charged with 100 mL of DD water in a 250-mL, round-bottom flask (RBF). About 0.40 g of sodium hydroxide was weighed and dissolved in 100 mL of DD water and slowly added to the 250-mL RBF under vigorous stirring conditions at 85°C. After 2 h of thorough mixing, the temperature of RBF was raised to 85°C, and stirring was continued for the next 48 h. At the end of the reaction, the content was filtered [the precipitate obtained was $Fe(OH)_2$] and dried at 110°C for 6 h. The same procedure was applied for the synthesis of ANI (1–5 wt % dispersant)-intercalated $Fe(OH)_2$.

Synthesis of the PVA/$Fe(OH)_2$ nanocomposites

PVA (1 g) was dissolved in 100 mL of DD water in a 250-mL RBF at 85°C for 2 h. After the complete dissolution of PVA in DD water, 1 wt % nanosized $Fe(OH)_2$ was added in a slow manner under vigorous stirring with nitrogen purging. After 3 h of vigorous stirring, the contents were poured onto a polyimide film and dried at room temperature for 24 h. A thin film was obtained after 24 h of removal of water molecules. Thus, the obtained PVA/$Fe(OH)_2$ nanocomposite film was subjected to various analytical characterizations.

Characterizations

FTIR spectra of the samples were recorded with a Shimadzu 8400 S FTIR spectrometer (Japan) by the KBr pelletization method. The corrected peak area (or integrated peak absorbance by a fitting procedure) was determined after proper baseline correction. The relative intensity (RI) was measured as follows:

$$\text{RI of the carbonyl peak} = \text{RI}_{[\text{C=O/CH}]} = A_{1733}/A_{844} \quad (1)$$

$$\text{RI of the terminal double bond} = \text{RI}_{[\text{C=C/CH}]\text{TD}} = A_{1578}/A_{844} \quad (2)$$

$$\text{RI of the midle double bond} = \text{RI}_{[\text{C=C/CH}]\text{MD}} = A_{1661}/A_{844} \quad (3)$$

where A indicates the corrected area of the peak, TD is the terminal double bond, and MD is the middle double bond. A double-beam ultraviolet–visible (UV–vis) spectrometer (Hitachi 3010 UV–vis spectrophotometer, Japan & USA) was used for the UV–vis spectral analysis of the nanocomposite sample solution. The photoluminescence (PL) study was carried out with an ElicoT spectrometer (India) with the excited wavelength of 260 nm. Thermogravimetric analysis (TGA) and differential scanning calorimetry (DSC) were carried out with an STA 409 instrument with a simultaneous TGA and DSC (MA, USA) analysis system at a heating rate of 10°C/min under a nitrogen atmosphere. The morphology and the phase identification of the products were characterized by field-emission scanning electron microscopy (FESEM; JSM 6300, JEOL, Japan; at 25 kV for SEM imaging) and XRD (XS08, Bruker, USA) with advanced instrument scanning from a 2θ value of 2 to 60° at a scanning rate of 2°/min. Furthermore, the structural analysis of nanosized $Fe(OH)_2$ was carried out by HRTEM (TEM 3010, JEOL, Japan).

RESULTS AND DISCUSSION

For the sake of convenience, the Results and Discussion section is subdivided into two parts discussing the characterizations of the nanosized $Fe(OH)_2$ and its hybrid and the characterizations of the PVA–$Fe(OH)_2$ nanocomposite. We analyze each one by one.

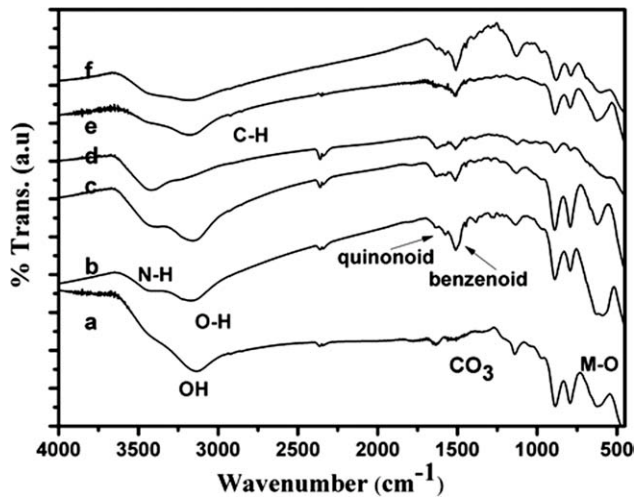

Figure 1 FTIR spectra of $Fe(OH)_2$ loaded with ANI at (a) 0, (b) 1, (c) 2, (d) 3, (e) 4, and (f) 5 wt %.

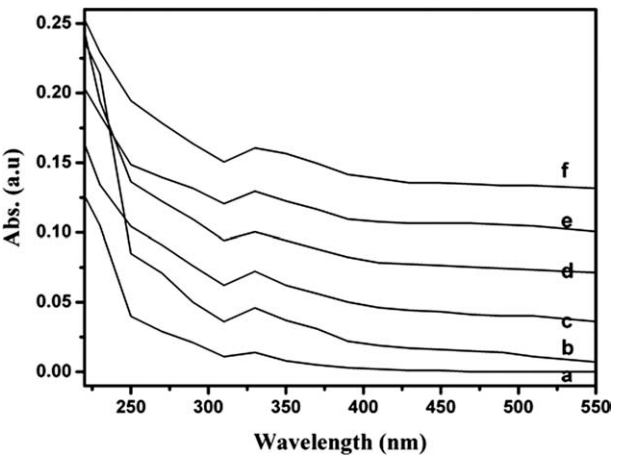

Figure 2 UV–vis spectra of (a) $Fe(OH)_2$, (b) $Fe(OH)_2$–1 wt % ANI, (c) $Fe(OH)_2$–3 wt % ANI, (d) $Fe(OH)_2$–5 wt % ANI, and (e) $Fe(OH)_2$–5 wt % ANI–PVA.

Characterizations of the nanosized $Fe(OH)_2$ and its hybrid

FTIR spectroscopy

Figure 1(a) shows the FTIR spectrum of pristine $Fe(OH)_2$. It showed three important characteristic peaks. Twin peaks appeared at 796 and 899 cm^{-1} and accounted for the metal hydroxide stretching vibration. A peak at 1629 cm^{-1} explained the bending vibration of water molecules attached to the $Fe(OH)_2$. The carbonate stretching appeared at 1155 cm^{-1}. The OH stretching vibration of $Fe(OH)_2$ appeared around 3250 cm^{-1}. Figure 1(b–f) shows the FTIR spectra of 1, 2, 3, 4, and 5 wt % ANI intercalated $Fe(OH)_2$. There were no prominent changes in the FTIR spectra. Because of the intercalation of ANI, some new peaks appeared in the FTIR spectra. The C—H symmetric and antisymmetric stretching vibration appeared around 2850 cm^{-1} as a small hump, the intensity of which was very low due to a lower percentage intercalation of ANI into the basal spacing of $Fe(OH)_2$. The benzenoid structure of ANI appeared at 1510 cm^{-1}. The thermally oxidized form of ANI (quinonoid form) appeared at 1650 cm^{-1}. The N—H stretching of ANI was assigned at 3421 cm^{-1}. Four peaks corresponding to benzenoid (1510 cm^{-1}), quinonoid (1650 cm^{-1}), N—H stretching (3421 cm^{-1}), and C—H stretching (2850 cm^{-1}) vibrations strongly supported the presence of ANI moieties[14–16] in the basal spacing of the layered structure of $Fe(OH)_2$.

UV–vis spectroscopy

Figure 2(a) shows the UV–vis spectrum of pristine $Fe(OH)_2$. A small hump at 326 nm confirmed the presence Fe^{2+} ions. Figure 2(b–f) shows the UV–vis spectra of 1–5 wt % ANI intercalated $Fe(OH)_2$ and 5 wt % $Fe(OH)_2$–ANI with the PVA nanocomposite system. One sharp peak appeared at a wavelength of 195 nm and corresponded to the chromophoric amino group of ANI intercalated into the basal spacing of $Fe(OH)_2$. This confirmed the presence of ANI in the basal spacing of $Fe(OH)_2$.

TGA profile

The thermal stability of $Fe(OH)_2$ was analyzed by TGA under an air atmosphere at a heating rate of 10°C/min. As shown in Figure 3(a), the thermogram showed a single-step degradation process. A weight loss step at 310°C showed that the dehydroxylation process started with the removal of water molecules. That is, at elevated temperatures, the hydroxyl groups of $Fe(OH)_2$ condensed with each other and removed the water molecules. Above 800°C, there was 87.5 wt % of $Fe(OH)_2$. Figure 3(b) showed the TGA of $Fe(OH)_2$ synthesized in the presence of 5 wt

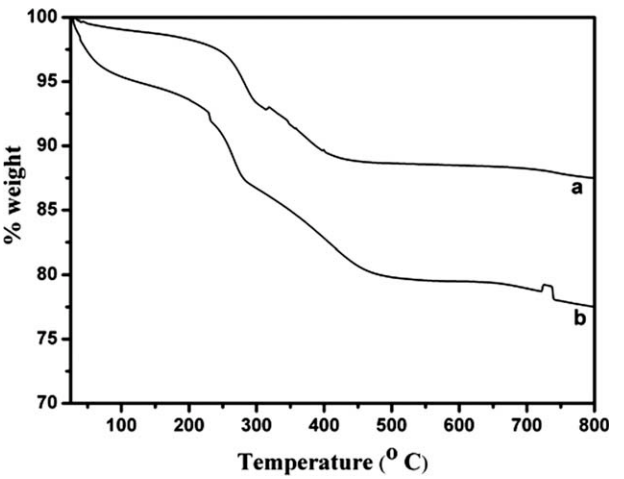

Figure 3 TGA of (a) $Fe(OH)_2$ and (b) $Fe(OH)_2$–5 wt % ANI.

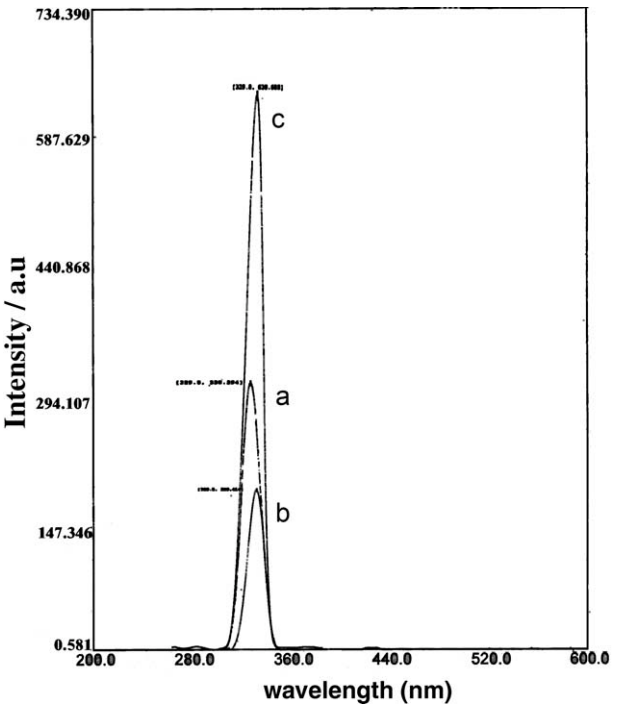

Figure 4 PL of (a) $Fe(OH)_2$, (b) $Fe(OH)_2$–5 wt % ANI, and (c) $Fe(OH)_2$–5 wt % ANI–PVA.

% ANI; the thermogram exhibited a two-step degradation process. The first minor weight loss up to 200°C was due to the removal of moisture, physisorbed and chemisorbed water molecules. Around 210°C, the dehydroxylation process started and extended up to 450°C. Above 800°C, approximately 75.5 wt % remained. This was due to the intercalation of ANI into the layered structure of $Fe(OH)_2$. Because of the amino intercalation into the $Fe(OH)_2$ structure, the thermal stability of $Fe(OH)_2$ above 800°C increased.

PL study

$Fe(OH)_2$ showed a sharp peak at a wavelength of 329 nm with the intensity of 330 mV in Figure 4(a). Figure 4(b) shows the PL of $Fe(OH)_2$ synthesized in the presence of 5 wt % ANI as a dispersing agent. In the presence of ANI, there was no change in the wavelength of $Fe(OH)_2$, but its intensity decreased to 209 mV. The sudden decrease in intensity was due to the presence of chromophoric amino groups of ANI in the basal spacing of $Fe(OH)_2$, that is, the intercalation reaction of ANI into the basal spacing of the layered $Fe(OH)_2$. The PL value for the PVA–5 wt % ANI-intercalated $Fe(OH)_2$ is shown in Figure 4(c). Here, the intensity was found to be 46.12 mV. The PL spectrum of $Fe(OH)_2$ appeared as a sharp peak at a wavelength of 330 nm. The PL of 5 wt % ANI-intercalated $Fe(OH)_2$ showed a sharp peak at 329 nm. In this case, there was no prominent change in the wavelength, but the intensity value slightly decreased. This was because of the intercalation of chromophoric amino groups into the layered structure of $Fe(OH)_2$. In the PVA–$Fe(OH)_2$–9 wt % ANI system, there was no change in the wavelength, but its intensity increased to 639 mV. The increase in intensity of the nanocomposite clearly explained the existence of interactions between PVA and the $Fe(OH)_2$–9 wt % ANI system. All of the samples were excited at 260 nm.

XRD profile

Figure 5(a) represented the XRD of pristine $Fe(OH)_2$. Peaks at 2θ values of 21 and 36° confirmed the presence of d_{021} and d_{101} crystal planes of $Fe(OH)_2$. Remaining peaks corresponded to the various crystal planes of $Fe(OH)_2$. The appearance of crystal peaks confirmed the crystalline nature of $Fe(OH)_2$. $Fe(OH)_2$ was synthesized in the presence of different weight percentages of ANI. $Fe(OH)_2$ synthesized in the presence of 1 wt % ANI [Fig. 5(b)] showed the same crystallinity, which was evidenced by a peak appearing at a 2θ value of 36°. $Fe(OH)_2$ synthesized in the presence of 3 wt % ANI [Fig. 5(c)] showed that there was decrease in the intensity of the crystalline peaks. $Fe(OH)_2$ synthesized in the presence of 5 wt % ANI [Fig. 5(d)] showed a spectrum with an ill crystalline peak. This implied that the synthesis of $Fe(OH)_2$ in the presence of a higher weight percentage of ANI (5 wt %) did not favor the crystalline nature of nanosized $Fe(OH)_2$. Our recent communications indicated that a higher weight percentage of dispersing agent leads to a reduction in the crystallinity of the nanomaterial.[17,18]

SEM analysis

Figure 6(a–d) shows the morphology of pristine $Fe(OH)_2$ as a nanotriangular-like morphology. Figure 6(a,d) indicates a fine, powderlike morphology. Figure 6(b) shows a broken, stonelike agglomerated particle morphology. Figure 6(c) exhibits a solidlike morphology. Figure 7(a,b) reveals the morphology of 1 wt % ANI-intercalated $Fe(OH)_2$. Figure 7(a) shows a spheroidal morphology, whereas Figure 7(b) indicates an agglomerated morphology. Here, also, a nanotriangular-like morphology was observed but with more numbers. This implied that lower concentration of dispersing agents such as ANI did not affect the morphology of $Fe(OH)_2$; however, it activated the formation of $Fe(OH)_2$. Figure 8(a–d) shows 5 wt % ANI-intercalated $Fe(OH)_2$. The microgram shows more smaller particles but an agglomerated structure, and also, it shows a distorted spherical morphology. Figure 8(a) shows a spherical particle morphology. Figure 8(b,c) indicates the ANI

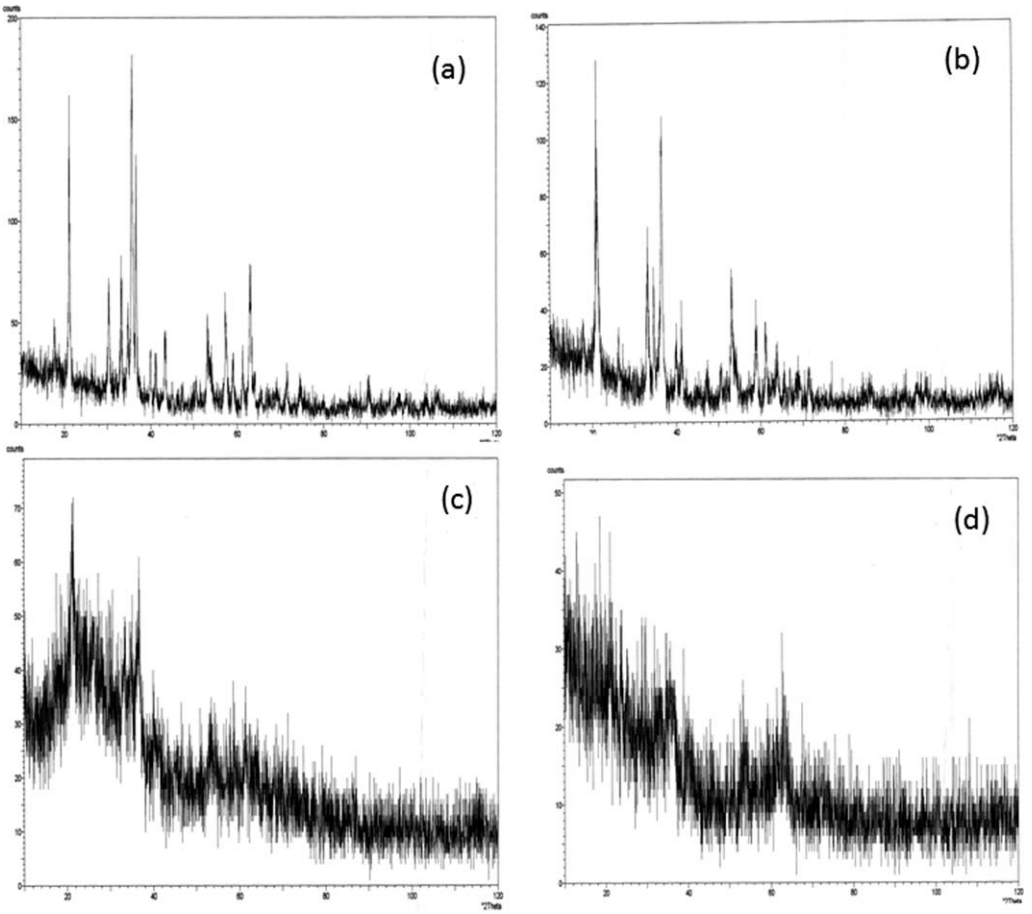

Figure 5 XRD of (a) $Fe(OH)_2$, (b) $Fe(OH)_2$–1 wt % ANI, (c) $Fe(OH)_2$–3 wt % ANI, and (d) $Fe(OH)_2$–5 wt % ANI.

intercalated morphology. Figure 8(d) confirms the linear crosslinking-like morphology. This implies that the synthesis of $Fe(OH)_2$ in the presence of a higher weight percentage of ANI led to the agglomerated structure, and hence, it was not a suitable weight percentage of dispersing agent for the synthesis of nanosized $Fe(OH)_2$. $Fe(OH)_2$ synthesized in the presence of ANI showed a distorted spheroidlike morphology. This urged us to determine the role of ANI during the synthesis of $Fe(OH)_2$.

HRTEM

The HRTEM topography of 5 wt % ANI-intercalated $Fe(OH)_2$ is shown in Figure 9. Because of the intercalation of ANI into the layered structure of $Fe(OH)_2$ [Fig. 9(a)], the layered structure of $Fe(OH)_2$ was distorted [Fig. 9(b)]. The size of the particles ranged from 10 to 50 nm. Because of the higher weight percentage of ANI, agglomeration [Fig. 9(c)] with a bundlelike morphology was observed. The selected area of electron diffraction (SAED) is given in Figure 9(d), which confirmed the semicrystalline nature of the hybrid. For the sake of comparison, the HRTEM image of pristine $Fe(OH)_2$ is shown in Figure 10. This shows a nanorod-like morphology [Fig. 10(a)] with an approximate size of 50 nm [Fig. 10(b,c)]. The SAED is given in Figure 10(d); this confirmed the crystalline nature of pristine $Fe(OH)_2$. In comparison, ANI-intercalated $Fe(OH)_2$ showed a distinct morphology with a size less of than 50 nm.

Characterizations of the nanosized PVA/$Fe(OH)_2$ nanocomposites

FTIR study

The added nanosized $Fe(OH)_2$ altered the structure of PVA via a surface catalytic effect. The PVA/$Fe(OH)_2$ nanocomposite was prepared in an aqueous medium with different weight percentages of $Fe(OH)_2$. During the course of the preparation of $Fe(OH)_2$ nanocomposites in the aqueous medium, there was a chance for the hydrolytic or thermolytic oxidation reaction, that is, olefin formation and a chain-scission reaction [Fig. 11(a–e)]. For the sake of comparison, the FTIR spectrum of pristine PVA is included in Figure 11(f). During the nanocomposite preparation, there must have been an interaction between $Fe(OH)_2$ and PVA. The existence of a secondary force of interaction between $Fe(OH)_2$ and OH groups of PVA must have appeared in the

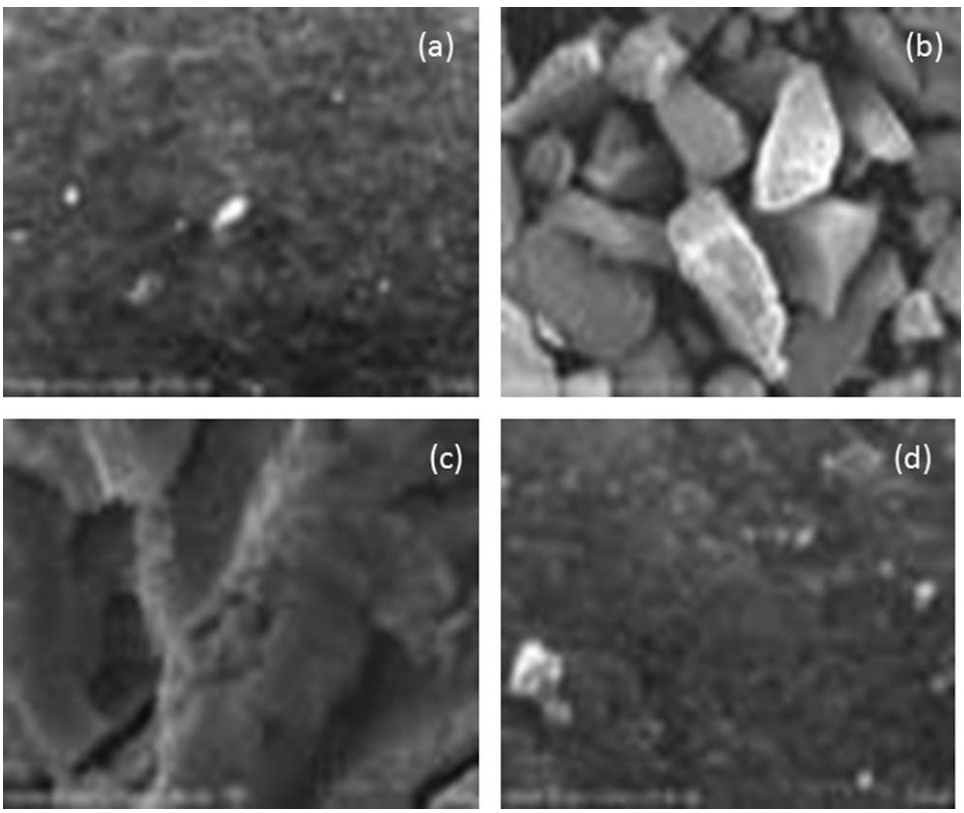

Figure 6 SEM images of pristine $Fe(OH)_2$.

wave-number range of 3550 cm^{-1}. However, in this investigation, because of the broad OH stretching of PVA, the existence of hydrogen bonding between $Fe(OH)_2$ and PVA did not clearly appear. In this investigation, we noted the effect of $Fe(OH)_2$ on the PVA structure. Here, we followed mainly two types of reaction during the nanocomposite formation: (1) the appearance of carbonyl stretching at 1730 cm^{-1} due to the conversion of a secondary alcoholic group into a ketone group and (2) because of the thermal and hydrolytic oxidation reaction, there was a chance for the formation of olefin bonds on the PVA backbone, that is, the formation of C=C bonds. The double bond may have been formed at the end of the polymer chain (1630 cm^{-1}) or at the middle of the polymer chain. Although the weight percentage of nanomaterial increased, the RIs of carbonyl formation and C=C formation also increased. With FTIR software, the change in the RIs of the carbonyl and C=C were quantitatively estimated, and the order of the formation reaction was determined. When the weight percentage of $Fe(OH)_2$ was

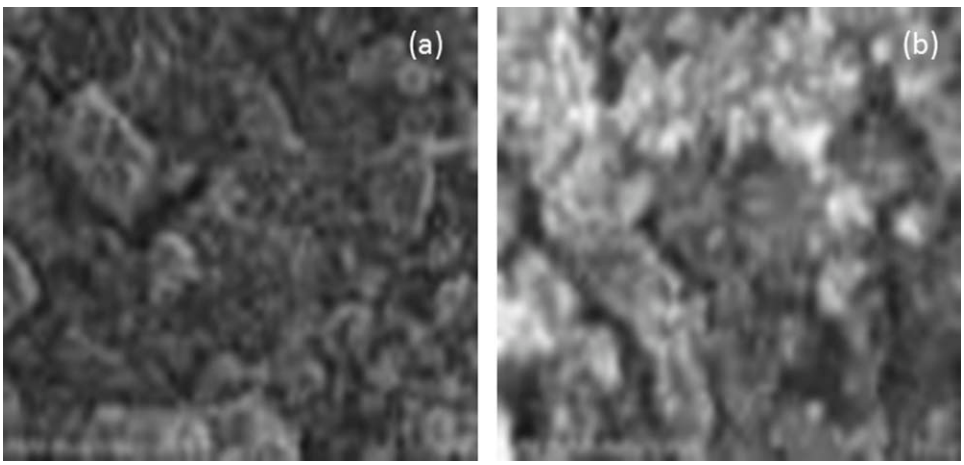

Figure 7 SEM images of $Fe(OH)_3$–1 wt % ANI.

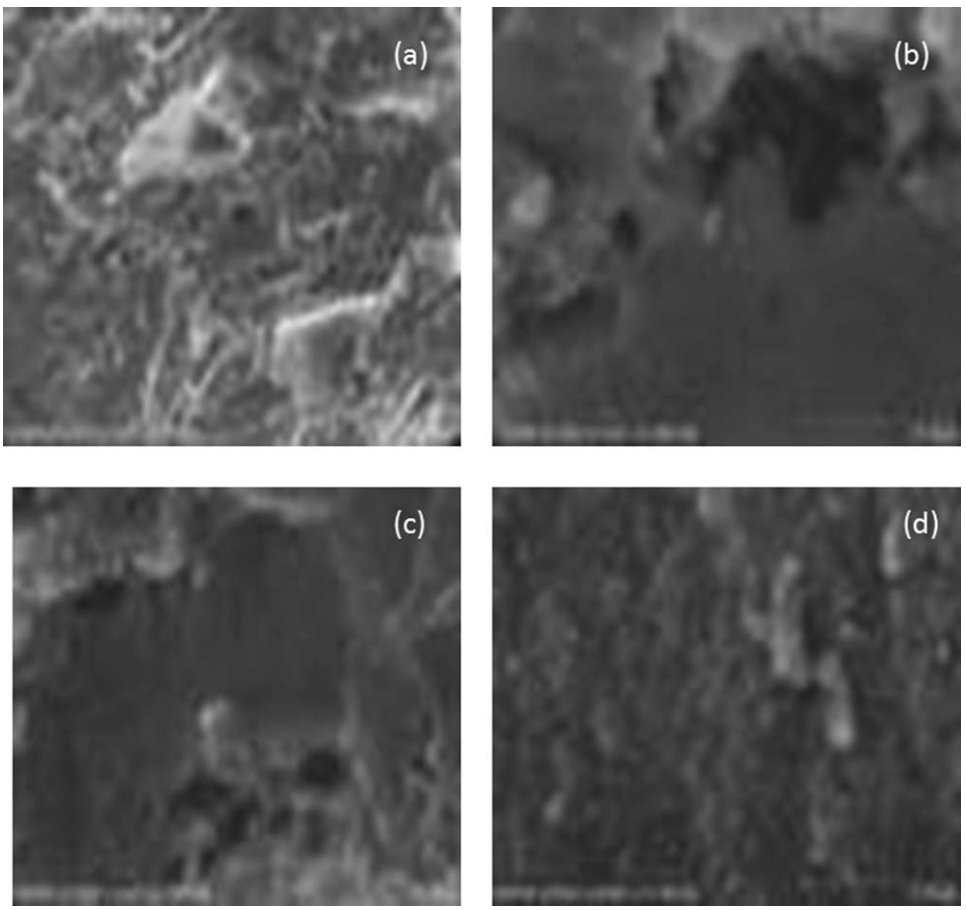

Figure 8 SEM images of $Fe(OH)_2$–5 wt % ANI.

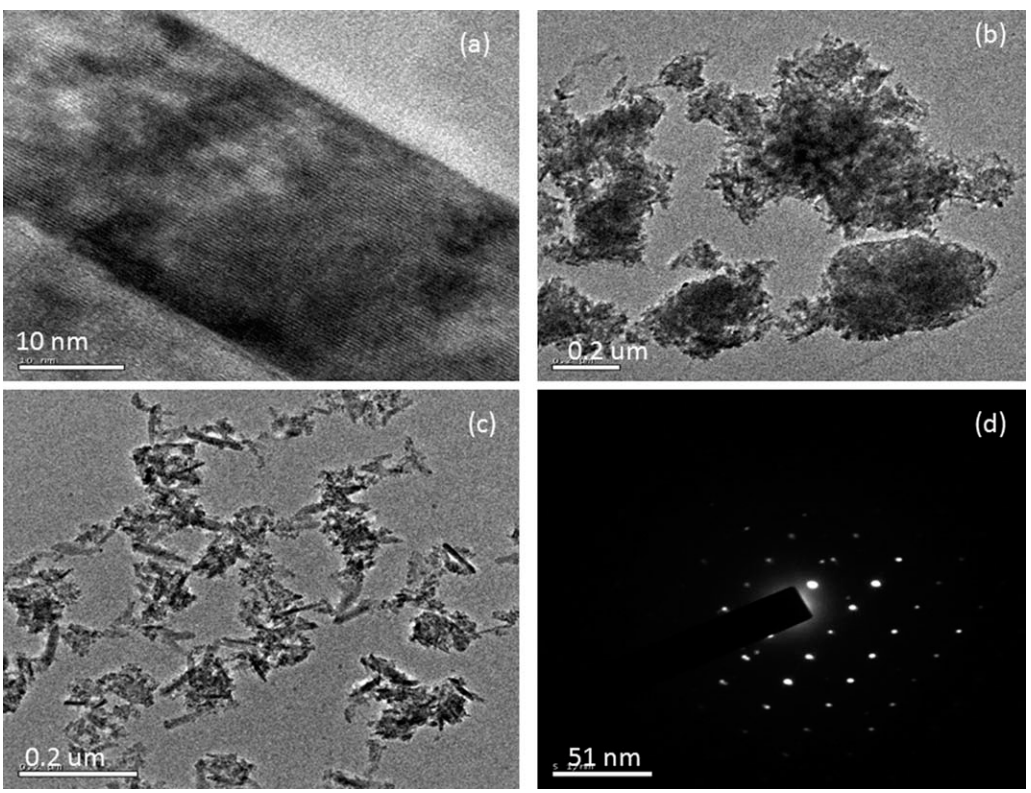

Figure 9 HRTEM of $Fe(OH)_2$–5 wt % ANI.

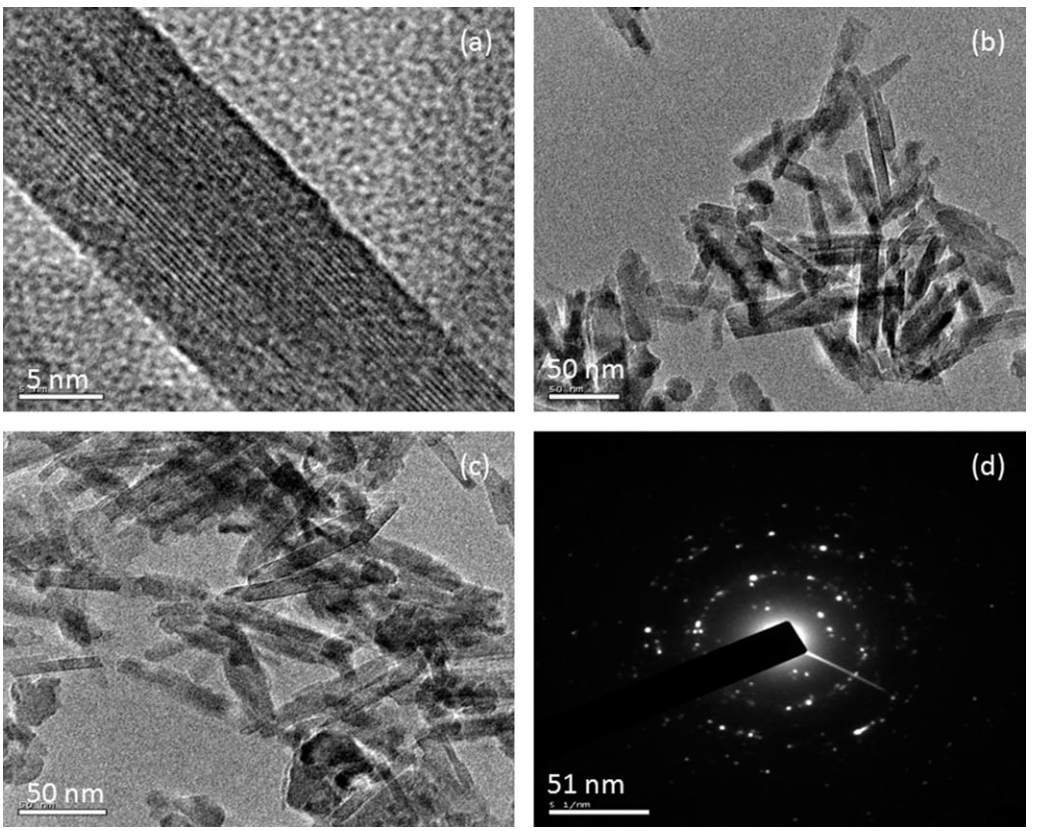

Figure 10 HRTEM of pristine $Fe(OH)_2$

increased from 1 to 9 wt %, the carbonyl group formation increased linearly. To determine the order of carbonyl group formation, the plot of log[wt % $Fe(OH)_2$] versus log($RI_{[C=O/CH]}$) [Fig. 12(a)] was drawn and found to be a straight line with a slope value of 0.97. The slope value indicated the 1.0 order of the carbonyl group formation reaction with respect to the weight percentage of $Fe(OH)_2$. Similarly, the C=C formation was quantitatively determined with the FTIR software. The plot of log [wt % $Fe(OH)_2$] versus log($RI_{[C=C/CH]TD}$) [Fig. 12(b)] followed a 0.90 order of reaction, and the plot of log[wt % $Fe(OH)_2$] versus log($RI_{[C=C/CH]MD}$) [Fig. 12(c)] followed a 0.94 order of reaction with respect to the weight percentage of $Fe(OH)_2$. These results indicate that the added nanosized $Fe(OH)_2$ accelerated the formation of double bonds, particularly, terminal double bonds, via a chain-scission process, which led to a reduction in the molecular weight of PVA. The decrease in the molecular weight is further under investigation in our laboratory. For the first time, we report here the amount of double bond formation during PVA/$Fe(OH)_2$ nanocomposite formation quantitatively through FTIR spectroscopy. In our earlier article, we reported the synthesis and characterization of the PVA/$Mg(OH)_2$ nanocomposite, in which the role of the nanomaterial on the structure and properties was explored by FTIR spectroscopy.[17,18] The ketone formation and alkene formation explained the role of nanosized $Fe(OH)_2$ on the structure of PVA. This was due to the active surface area of the nanosized $Fe(OH)_2$.

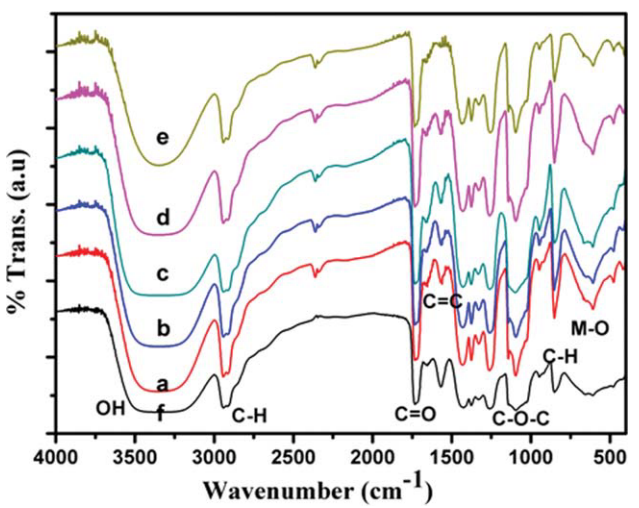

Figure 11 FTIR spectra of PVA loaded with $Fe(OH)_2$ at (a) 1, (b) 3, (c) 5, (d) 7, (e) 9, and (f) 0 wt %. [Color figure can be viewed in the online issue, which is available at www.interscience.wiley.com.]

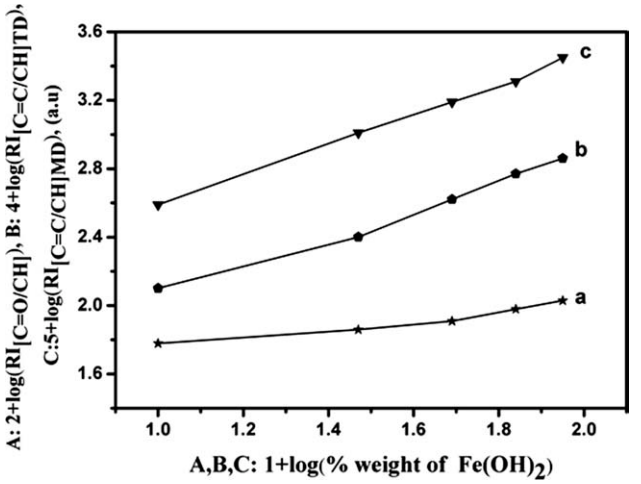

Figure 12 Effect of the weight percentage of $Fe(OH)_2$ on the (a) $RI_{[C=O/CH]}$, (b) $RI_{[C=C/CH]TD}$, and (c) $RI_{[C=C/CH]MD}$ (weight of PVA = 1.0 g, time = 3 h, temperature = 80°C).

TGA history

Figure 13 (Table I) shows the TGA thermogram of PVA loaded with $Fe(OH)_2$ from 1 to 9 wt %. The thermogram shows a three-step degradation process. The first minor weight loss step, up to 150°C, was due to the removal of moisture and physisorbed water molecules. The second major weight loss step was associated with the degradation of the PVA backbone. The degradation was extended up to 350°C. The third minor weight loss step around 425°C corresponded to the dehydroxylation process of $Fe(OH)_2$. The appearance of this weight loss process confirmed the existence of interactions between PVA and $Fe(OH)_2$, that is, the existence of secondary forces of attraction between the OH groups of PVA with $Fe(OH)_2$. Another interesting point noted here was that, when the weight percentage of $Fe(OH)_2$ was increased, the weight percentage residue remaining at 750°C increased simultaneously. The char-forming capability of PVA increased slightly. This was in accordance with our earlier article.[18]

TABLE I
TGA of PVAs Loaded with Different Weight Percentages of $Fe(OH)_2$

System	Weight percentage (wt %) at				
	200°C	300°C	400°C	500°C	700°C
PVA–1 wt % $Fe(OH)_2$	90.4	40.5	32.7	21.1	12.5
PVA–3 wt % $Fe(OH)_2$	88.5	54.9	35.8	23.1	15.7
PVA–5 wt % $Fe(OH)_2$	89.7	52.5	35.2	26.6	16.2
PVA–7 wt % $Fe(OH)_2$	88.3	57.8	35.1	27.3	18.5
PVA–9 wt % $Fe(OH)_2$	91.2	58.8	38.3	30.2	21.7

DSC study

The DSC results of PVA loaded with different weight percentages of $Fe(OH)_2$ are shown in Figure 14. The de-watering temperature ($T_{d.w}$) of the PVA/$Fe(OH)_2$ nanocomposite appeared at 125°C. The α-transition temperature (T_α) appeared at 202°C. The melting temperature appeared at 320°C. When the weight percentage of $Fe(OH)_2$ was increased from 1 to 9 wt %, the melting temperature value also simultaneously increased. This was because of chelation between the Fe(II) and OH groups of PVA. During nanocomposite formation, the OH groups of PVA must have been overcoated on the $Fe(OH)_2$. Our experimental outcomes were in accordance with those of previous reports.[17–19]

HRTEM analysis of the PVA-coated $Fe(OH)_2$

Figure 15(a) shows the HRTEM image of the PVA/$Fe(OH)_2$ nanocomposite system. The image indicates that part of its layered structure was broken after the nanocomposite was made with PVA. Part of the

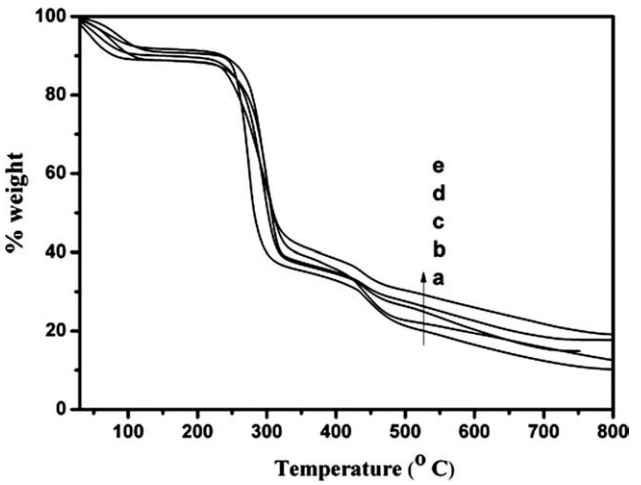

Figure 13 TGA of PVA loaded with $Fe(OH)_2$ at (a) 1, (b) 3, (c) 5, (d) 7, and (e) 9 wt %.

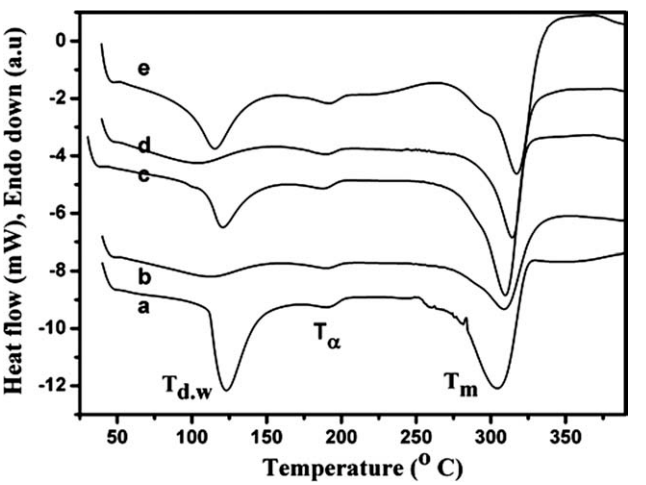

Figure 14 DSC results of PVA loaded with $Fe(OH)_2$ at (a) 1, (b) 3, (c) 5, (d) 7, and (e) 9 wt %.

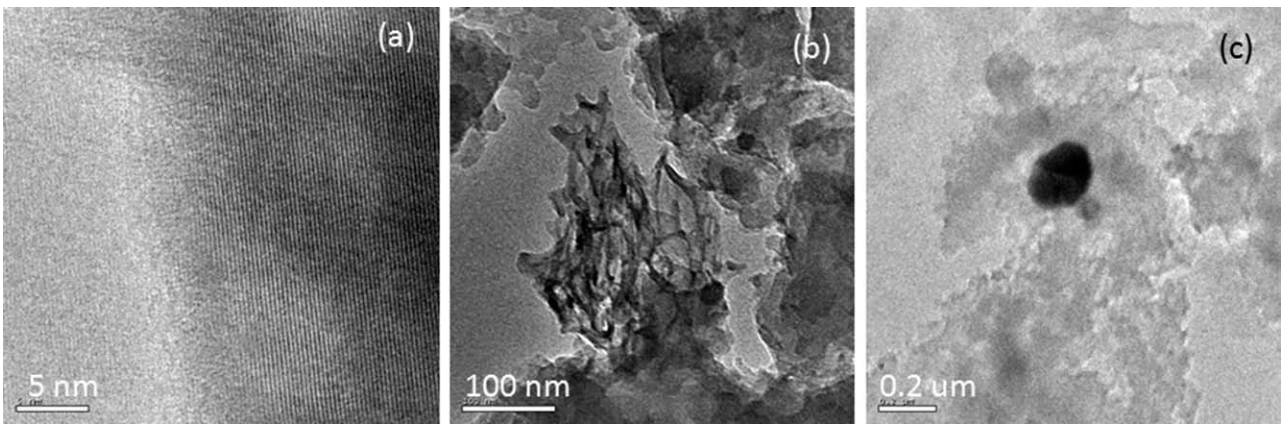

Figure 15 HRTEM images of PVA loaded with 5 wt % $Fe(OH)_2$.

layered structure of $Fe(OH)_2$ was not disturbed with the length of 20–25 nm. Figure 15(b) represents the uniform distribution of 20-nm-sized $Fe(OH)_2$ nanoparticles on the PVA matrix without agglomeration by showing sphere morphology. Figure 15(c) confirms the agglomerated $Fe(OH)_2$ with the size of 200 nm. By analyzing Figure 15, we concluded that, even after nanocomposite formation with PVA, part of the layered structure of $Fe(OH)_2$ was maintained with its sphere morphology.

CONCLUSIONS

In summary, nanosized $Fe(OH)_2$ was synthesized by a coprecipitation method with the help of ANI as a self-assembler, and this gave us favorable results. FTIR confirmed the presence of metal hydroxide stretching in the $Fe(OH)_2$–ANI hybrid. The appearance of the d_{021} plane in the XRD of $Fe(OH)_2$ confirmed the crystalline nature of $Fe(OH)_2$. TGA showed thermal stability, even at 800°C. The 5 wt % ANI-intercalated $Fe(OH)_2$ showed a distorted nanorod-like morphology with a size of 10–50 nm; the pristine $Fe(OH)_2$ also showed the same morphology. SEM implied that a nanospheroid morphology of pristine $Fe(OH)_2$, and the higher weight percentage ANI-intercalated $Fe(OH)_2$ had an agglomerated structure. The UV–vis spectrum declared that presence of Fe^{2+} ions at 326 nm, and the presence of amino-group-intercalated $Fe(OH)_2$ showed a sharp peak at 195 nm, the intensity of which increased along with increasing weight percentage of ANI. PL implied that ANI-intercalated $Fe(OH)_2$ showed a lesser intensity than the pristine $Fe(OH)_2$ and an increase in the PL intensity with the PVA/$Fe(OH)_2$ nanocomposite. The order of carbonyl, terminal, and middle double-bond formation in PVA followed a 1.0 order of reaction with respect to weight percentage of $Fe(OH)_2$.

References

1. Erlebacher, J.; Aziz, M. J.; Karma, A.; Dimitrov, N. Nature 2001, 410, 450.
2. Neuberger, T.; Hofman, H.; van Rechenberg, B. J Magn Magn Mater 2005, 293, 483.
3. Wang, S. H.; Shi, X.; Cao, Z.; Bi, X.; Baker, J. R., Jr. Adv Funct Mater 2007, 17, 3043.
4. Zhang, L.; Chen, L.; Wan, Q. H. Chem Mater 2008, 20, 3345.
5. Ohtsuka, K.; Suda, M.; Ono, M. Bull Chem Soc Jpn 1988, 61, 815.
6. Jiao, C. M.; Wang, Z. Z.; Chen, X. L.; Hu, Y. J Appl Polym Sci 2008, 107, 2626.
7. Shi, Q. X.; Lu, R. W.; Zhang, Z. X.; Zhao, D. F. Chin Chem Lett 2006, 17, 1045.
8. Jung, S. J.; Amal, R.; Jo, Y. M. J Ind Eng Chem 2001, 7, 92.
9. Capponi, F.; Sarrosi, M.; Souza, M. L.; Rubio, J. Int J Miner Process 2006, 79, 167.
10. Hansen, B.; Koch, C. B.; Taylor, R. M. J Solid State Chem 1994, 113, 46.
11. Iijima, M.; Yonemochi, Y.; Tsukada, M.; Kamiya, H. J Colloid Inter Sci 2006, 298, 202.
12. Schwartz, A. W.; Ongel, L. E. J Mol Evol 1985, 2, 299.
13. Yeung, S. C. F.; Eaton, D. R. Can J Chem 1985, 63, 3378.
14. Yelilarasi, A.; Juliat Latha Jayakumari, J.; Dhanalakshmi, V.; Anbarasan, R. Spectrochim Acta A 2009, 74, 1229.
15. Yelilarasi, A.; Juliat Latha Jayakumari, J.; Dhanalakshmi, V.; Anbarasan, R. Polym Polym Compos 2009, 17, 397.
16. Anbarasan, R.; Gopalan, A.; Vasudevan, T. Polym News 1999, 24, 391.
17. Fathima Parveen, M.; Umpathy, S.; Anbarasan, R. Nano Rev Rep 2009, 4, 147.
18. Parveen, M. F.; Umpathy, S.; Dhanalalakshmi, V.; Anbarasan, R. J Mater Sci 2009, 44, 5852.
19. Parveen, M. F.; Umpathy, S.; Anbarasan, R. Compos Int, to appear.